

A Three Micron Survey of the Chamaeleon I Dark Cloud ¹

Scott J. Kenyon

Smithsonian Astrophysical Observatory, 60 Garden Street, Cambridge MA 02138

skenyon@cfa.harvard.edu

and

Mercedes Gómez

Observatorio Astronómico de Córdoba, Laprida 854, 5000 Córdoba, Argentina

mercedes@oac.uncor.edu

to be published in the

Astronomical Journal

May 2001

ABSTRACT

We describe an L -band photometric survey of ~ 0.5 deg² of the Cha I dark cloud. The survey has a completeness limit of $L < 11.0$. Our survey detects 124 sources, including all known pre-main sequence stars with $L \leq 11$. The fraction of sources with near-IR excess emission is $58\% \pm 4\%$ for $K = 9\text{--}11$. Cha I sources have bluer $H - K$ and $K - L$ colors than pre-main sequence stars in Taurus-Auriga. These sources also have a strong correlation between $\text{EW}(\text{H}\alpha)$ and $K - L$. Stars with $K - L \leq 0.6$ have weak $\text{H}\alpha$ emission; stars with $K - L \geq 0.6$ have strong $\text{H}\alpha$ emission. Because many Cha I sources are heavily reddened, this division between weak emission T Tauri stars and classical T Tauri stars occurs at a redder $K - L$ than in Taurus-Auriga.

Subject headings: ISM: individual (Chamaeleon I) — stars: formation — stars: pre-main sequence — infrared: stars

¹Based on observations obtained with the SPIREX/Abu system in Antarctica. SPIREX/Abu operated for the 1999 observing season under agreement between the National Optical Astronomy Observatories (NOAO) and the Center for Astrophysical Research in Antarctica (CARA).

1. Introduction

Pre-main sequence T Tauri stars (TTS) often display excess infrared (IR) emission compared to a normal stellar photosphere. The circumstellar material which produces this emission has temperatures ranging from ~ 50 K up to ~ 2000 K (e.g., Rucinski 1985; Rydgren & Zak 1987). Large disks surrounding TTS can produce these temperatures by reprocessing stellar radiation or by material flow through the disk at rates of $1\text{--}10 \times 10^{-8} M_{\odot} \text{ yr}^{-1}$ (Bertout et al. 1988; Kenyon & Hartmann 1987). Disks can also produce the eruptions observed in pre-main sequence stars (e.g., Hartmann & Kenyon 1996). After years of detailed comparisons between data and disk models for the energy distributions and other physical properties of T Tauri stars, recent images from *Hubble Space Telescope* (e.g., Burrows et al. 1996; Ghez et al. 1997; Krist et al. 2000) and ground-based radio interferometers (e.g., Koerner et al. 1993; Wilner et al. 1996, 2000) dramatically confirmed that circumstellar disks are responsible for the IR excesses of pre-main sequence stars.

Measuring the evolution of disks surrounding pre-main sequence stars is important for understanding the evolution of the central star and the evolution of the disk into a planetary system (e.g., Hartmann et al. 1998; Lada 1999). Large surveys of nearby star-forming regions are needed to derive the samples of pre-main sequence stars required for estimates of stellar ages and disk properties (e.g., Kenyon & Hartmann 1995). Modern instruments at optical, near-IR, mid-IR, and X-ray wavelengths can now provide such samples fairly routinely.

Here we report results of an *L*-band photometric survey of the central portion of the Cha I dark cloud, an active star-forming region with more than 150 pre-main sequence stars (e.g., Lawson et al. 1996). Our goal is to constrain properties of the disks in these pre-main sequence stars using the *K* – *L* color index for a complete sample of stars selected at *K* and *L*. This survey complements our recent *JHK* imaging survey (Gómez & Kenyon 2001) and other near-IR surveys (Cambrésky et al. 1998; Persi et al. 1999; Oasa et al. 1999). The new *L*-band data also provide a needed link between near-IR surveys and mid-IR and far-IR surveys with *ISO* and *IRAS* data (e.g., Persi et al. 2000; Baud et al. 1984).

We describe the *L*-band survey in §2, analyze the data in §3, and conclude with a brief summary in §4.

2. Observations and Data Analysis

We acquired *L*-band photometry of Cha I sources and standard stars using the South Pole Infrared Explorer (SPIREX) during the 1999 March to October observing season. The SPIREX 60 cm telescope developed by CARA for observations at the South Pole was equipped with the NOAO/KPNO Abu infrared camera (Fowler et al. 1998), which includes a first generation 1024×1024 InSb detector array. With a scale of $0''.6 \text{ pixel}^{-1}$, the Abu field-of-view was $\sim 10' \times 10'$ for these observations. We divided the Cha I field into a 12×5 grid roughly coincident with our

coverage from a *JHK* survey using CIRIM at the Cerro Tololo Interamerican Observatory (Gómez & Kenyon 2001). Here we describe photometry derived from the central $100' \times 20'$ of the grid, acquired on 17 and 18 July 1999. Registration problems prevented us from matching other *L*-band sources to *JHK* sources from the CTIO survey.

J. Kastner and collaborators at the Rochester Institute of Technology (RIT) performed the initial data reduction of the SPIREX/Abu images. They developed a library of IDL processing algorithms to flat-field and to register five dithered images per target field. They also derived sky conditions each night, using measured backgrounds and standard stars. Our observations were generally made in good conditions with below-average backgrounds².

We derived calibrated *L*-band photometry of Cha I sources using routines in IRAF³. We used IRAF PHOT with an 8 pixel aperture to derive the standard star calibration and photometry of Cha I sources. This aperture encircles 95% or more of the light of all sources, based on measurements of the point-spread function for standard stars and bright Cha I sources. We used measured backgrounds and observations of 8–9 standard stars on 17–21 July 1999 to establish the extinction correction for the Earth’s atmosphere and the photometric zero-point. We adopted *L*-band magnitudes for the standards from the SPIREX/Abu web page cited previously. The *L*-band calibration and extinction correction are accurate to $\pm 10\%$ or better. Comparisons of our Cha I photometry with previous measurements suggest a typical error of ± 0.05 mag for bright sources with $L = 7-8$, ± 0.10 mag for sources with $L = 9-11$, and ± 0.20 mag for sources at the detection limit, $L \geq 11$.

Table 1 lists *L* magnitudes and $K - L$ colors for 124 *L*-band sources detected in our survey. The J2000.0 coordinates and the *JHK* data in Table 1 are from the CIRIM survey. To make reliable matches for the *L*-band sources, we derived preliminary coordinates from the *L*-band images using the WCSTools routines⁴. We adopted the nominal pixel scale and chose a rough center for each frame by eye. We made one iteration of the center to minimize the average deviation between *JHK* and *L* coordinates for the 3–6 sources with $L \leq 10$ in each image, and then matched fainter sources one-by-one. The small number of sources per image prevented us from making a more accurate fit for the plate solution on most images.

We made several tests to estimate the completeness limit for the SPIREX/Abu survey. Figure 1 compares counts in half magnitude bins (left panel) with number counts for the entire population of known pre-main sequence stars in Cha I (right panel). Both sets of counts rise monotonically to $L = 11$ and then turn over. These results suggest a completeness limit of $L = 10.75 \pm 0.25$. To confirm this estimate, we used K and $H - K$ from our CIRIM survey of Cha I (Gómez & Kenyon 2001) to predict *L* magnitudes assuming $K - L \approx H - K \pm \delta m$. We tried many Monte Carlo trials

²A detailed description can be found at: <http://pipe.cis.rit.edu/index.html>

³IRAF is distributed by the National Optical Astronomy Observatory, which is operated by the Association of Universities for Research in Astronomy, Inc. under contract to the National Science Foundation.

⁴Available at <ftp://cfa-ftp.harvard.edu/pub/gsc/WCSTools>

for random δm in the range 0.1–0.4 mag. We detected all CIRIM sources with $K < 10.5$ in our survey region. For fainter sources, this test predicts 10 undetected L -band sources with $K < 12$ independent of the adopted error, δm . Two of these, ISO 103 and 110826–765559 from Gómez & Kenyon (2001), have $K = 10.5$ – 11.0 and $H - K < 0.5$; the rest have $K > 11$ and $H - K < 1$ and should lie close to our detection limit of $L = 11$. Thus, our survey is essentially complete for stars with $L < 11$, which are comparable in brightness to the faintest known pre-main sequence stars in the cloud.

3. Analysis

Our L -band survey of 124 sources covers a modest fraction, $\sim 0.5 \text{ deg}^2$, of the Cha I star-forming region. We recover all previously known near-IR sources in the region, including 15 discovered in our deep JHK survey with CIRIM at CTIO (Gómez & Kenyon 2001). Only ~ 40 stars in this sample have reliable $H\alpha$ equivalent width measurements; fewer than half of the sample have reliable spectral types. A complete analysis thus requires additional optical spectra for the entire sample, which is beyond the scope of this paper. Here, we consider the near-IR color-color diagrams (§3.1), the fraction of sources with near-IR excesses (§3.2), and a correlation of two indicators of disk accretion, $K - L$ and the equivalent width of $H\alpha$ (§3.3).

3.1. Color-color diagrams

Figure 2 shows, side by side, the $J - H$ vs $H - K$ and $J - H$ vs $K - L$ color-color diagrams for all previously known young stellar objects in the Cha I cloud. We compiled from the literature L magnitudes for known pre-main sequence stars missed by our L -band survey (due mainly to frame registration problems) or saturated in our images (Glass 1979; Gauvin & Strom 1992; Prusti, Whittet & Wesselius 1992; Lawson et al. 1996). We used the online Catalog of Infrared Observations⁵ to check the completeness of this sample. The dot-dashed lines indicate the expected locus of reddened stars with the intrinsic colors of normal main sequence stars (Bessell & Brett 1988; Gómez & Kenyon 2001). Stars lying outside this band have near-IR excesses from circumstellar dust (Allen 1972; Hyland 1980; Hyland et al. 1982). The $J - H$ vs $K - L$ diagram shows more stars with near-IR excess than the $J - H$ vs $H - K$ diagram. The $3 \mu\text{m}$ data are less compromised by interstellar reddening and provide more contrast relative to photospheric emission from the central star than shorter wavelength observations (see Haisch, Lada, & Lada 2000; Lada et al. 2000; Kenyon & Hartmann 1995, and references therein).

Figure 3 compares the frequency distribution of the $K - L$ color index in Cha I with the distribution in the Taurus-Auriga dark cloud (Kenyon & Hartmann 1995). We show two distributions

⁵Available at <http://ircatalog.gsfc.nasa.gov>

of Cha I stars, our SPIREX/Abu sample and a combined sample using data compiled from the literature to supplement SPIREX/Abu data. These two distributions have the same median $K - L$, 0.57 (SPIREX/Abu sample) and 0.58 (combined sample), and a probability of more than 99.9% of being drawn from the same parent distribution according to a K-S test. The Cha I frequency distribution consists of a single peak at $K - L \approx 0.4-1.6$ and a red tail which extends to $K - L \approx 2.2$. The small peaks at $K - L \approx 1.1$ and $K - L \approx 1.5$ are due to small number statistics according to a K-S test. The Taurus-Auriga distribution has two peaks, weak emission T Tauri stars (WTTs) with $K - L \leq 0.2$ and classical T Tauri stars (CTTs) with $K - L \approx 0.8-1.0$ (Kenyon & Hartmann 1995). The CTTs peak in Taurus-Auriga has a broad shoulder extending to $K - L \approx 3$ which includes many class I protostars.

Two main differences between the Cha I and Taurus-Auriga pre-main sequence stars produce the different $K - L$ frequency distributions. The Taurus-Auriga cloud has many more protostars with $J - H \geq 3$ and $H - K \approx K - L \geq 2$ than does Cha I. The Cha I population also does not show a peak at $K - L \leq 0.2$, because WTTs in Cha I are more heavily reddened than WTTs in Taurus-Auriga. For stars with accurate spectral types, the median optical reddening is $A_V \sim 0.6$ mag for Taurus-Auriga WTTs (Kenyon & Hartmann 1995) and $A_V \sim 1.6$ mag for Cha I WTTs (e.g., Lawson et al. 1996). Our near-IR color-color diagrams suggest a population of fainter and much more heavily reddened Cha I WTTs with $A_V \sim 5-10$. Optical or near-IR spectra of these sources are necessary to test this prediction.

Despite the larger reddening, the median near-IR colors of young stars in Cha I are bluer than the median near-IR colors of young stars in Taurus-Auriga. We derive a median $K - L$ of $0.58^{+0.35}_{-0.16}$ for Cha I sources and $0.73^{+0.33}_{-0.48}$ for Taurus-Auriga stars. The error bars indicate the inter-quartile ranges for each sample. The difference in the observed $K - L$ color has a 2σ significance according to a K-S test. Estimating the intrinsic color difference between Cha I and Tau-Aur sources is difficult, because most of the Cha I stars do not have measured spectral types. Adopting K0-M6 spectral types for these stars, we can estimate A_V from the observed near-IR colors and make a crude comparison with Tau-Aur sources with measured A_V . This exercise increases the significance of the color difference to $3-4\sigma$, depending on the very uncertain reddening correction. Acquiring good spectral types for these Cha I sources would allow a better test.

The $K - L$ frequency distribution in Cha I has some features in common with the frequency distribution in ρ Oph (Figure 3). We compiled JHK data from Barsony et al. (1997) and L data from the Catalog of Infrared Observations (see Elias 1978; Wilking & Lada 1983; Comerón et al. 1993, and references therein). Both clouds have a single, well-defined peak at $K - L < 1$. In ρ Oph, this peak consists of heavily reddened WTTs and a few moderately reddened CTTs. Unlike Cha I, ρ Oph has a population of very red protostars as in the Taurus-Auriga cloud. The second peak in the ρ Oph distribution at $K - L \approx 2.0-2.5$ has a $2-3\sigma$ significance according to a K-S test. Some of the stars in this peak are heavily reddened CTTs.

3.2. Near-IR excesses

In the current picture of star formation, young stars evolve from deeply embedded protostars into CTTs and then into WTTs before arriving on the main sequence. The CTTs are pre-main sequence stars surrounded by a circumstellar disk; the flow of material through the disk onto the star produces an optical/ultraviolet excess and an IR excess over photospheric emission from the central star. Reprocessing of stellar radiation by the disk also produces some of the IR excess (e.g., Kenyon & Hartmann 1987; Chiang & Goldreich 1997). The WTTs do not have excess emission, either because the disk has dispersed or because the disk emits too little radiation to produce an excess.

The ‘disk fraction’ is an interesting parameter in this picture. The disk fraction is the fraction of T Tauri stars with IR excess emission. Because long wavelength near-IR colors provide more contrast relative to emission from the stellar photosphere, recent studies have used the $K - L$ color to measure the disk fraction (e.g., Haisch et al. 2000). Longer wavelength colors such as $K - N$ or $K - Q$ would probably provide a better measure (e.g., Kenyon & Hartmann 1995), but these data are difficult to obtain for large samples of pre-main sequence stars with current technology.

To estimate the number of sources with $K - L$ excesses in Cha I, we employ a Monte Carlo simulation to account for uncertainties in the $K - L$ colors and the uncertainty in the slope of the reddening band. To construct the simulation, we begin with $(J - H, K - L)$ pairs for our sample, $(J - H, K - L)$ colors of normal main sequence stars from Kenyon & Hartmann (1995), and an adopted slope for the reddening law, $E_{J-H}/E_{K-L} = 1.88$ from Bessell & Brett (1988). We adopt an error of ± 0.05 in the slope of the reddening law (see Bessell & Brett 1988; Kenyon et al. 1998; Gómez & Kenyon 2001). For each Monte Carlo trial, we replace each color index with an artificial color index c'_i ,

$$c'_i = c_i + e_i g_i , \quad (1)$$

where c_i is the observed color index, e_i is the error in the color index, and g_i is a normally distributed deviate with zero mean and unit variance (Press et al. 1992). The reddening law for each trial is

$$E_{J-H}/E_{K-L} = 1.88 + 0.05g_i , \quad (2)$$

We then derive the fraction of sources which lie to the right of the reddening band in the color-color diagram. After 10,000 such trials, we evaluate the median fraction of IR excess sources and the inter-quartile range of the distribution. This simulation allows us to estimate the error in the fraction of IR excess sources and to evaluate the sensitivity of this fraction to uncertainties in the near-IR colors, the intrinsic main sequence star colors, and the slope of the reddening band.

Our set of Monte Carlo trials results in an observed fraction of sources with $K - L$ excess emission, $58\% \pm 4\%$. The 1σ uncertainty includes the uncertainty in the observed colors and the

slope of the reddening law. This fraction does not depend on errors in the intrinsic colors of main sequence stars used to define the reddening band. The fraction of IR excess sources is sensitive to the real slope of the reddening band. In general, there are fewer near-IR excess sources if the slope of the reddening law is shallower than the adopted law. In practice, most Cha I sources with $K - L$ excesses lie well away from the reddening band. Unless the real slope of the reddening law is 3σ or more shallower than the adopted slope, this uncertainty does not affect our result significantly.

The disk fraction of $58\% \pm 4\%$ in Cha I is smaller than disk fractions estimated for Taurus-Auriga, 69%, the Trapezium cluster, $80\% \pm 7\%$ (Lada et al. 2000), and NGC 2024, $86\% \pm 8\%$ (Haisch et al. 2000). Cha I has fewer class I protostars than does Taurus-Auriga (Kenyon & Hartmann 1995); Cha I probably has fewer protostars than NGC 2024 and the Trapezium cluster. We suspect that Cha I has fewer protostars and a smaller disk fraction, because it contains a larger fraction of older pre-main sequence stars than Taurus-Auriga, the Trapezium cluster, or NGC 2024 (Kenyon & Hartmann 1995; Lawson et al. 1996; Hartmann et al. 1998; Haisch et al. 2000; Lada et al. 2000). Measurement of a smaller disk fraction, $65\% \pm 8\%$, in the older cluster IC 348 supports this conclusion (Haisch, Lada & Lada 2001). Age estimates for newly discovered pre-main sequence stars in Cha I and comparisons with other star-forming regions are needed to confirm relationships between stellar age and disk fraction.

To examine the disk fraction and IR excesses of Cha I sources in more detail, we considered the $K - m(6.7)$ and $K - m(14.3)$ colors derived from our data and data from the ISO mission (Nordh et al. 1996; Persi et al. 2000). With the calibration of Olofsson et al. (1999), we constructed color-color diagrams using our $J - H$ and $K - L$ colors to search for correlations between near-IR and mid-IR excesses. As expected, WTTs have bluer $K - m(6.7)$ and $K - m(14.3)$ colors than CTTs. We found weak ($1-2\sigma$) evidence for a deficit of Cha I sources with $K - m(14.3) \approx 3-4$. The Taurus-Auriga cloud has a considerable deficit of sources with $K - N \approx 0.75-2.25$, producing a pronounced gap between the CTTs and the WTTs in this cloud (see Kenyon & Hartmann 1995, and references therein). Although this deficit is interesting, the Cha I sample is too small and too heavily reddened to make a strong case for a deficit similar to the one observed in Taurus-Auriga. Future mid-IR observations with the Space Telescope Infrared Facility and other instruments will yield better statistics on the distribution of mid-IR excesses in Cha I sources.

3.3. $H\alpha$ Equivalent Widths

In most circumstellar disk models, the disk emits in the IR while an accretion stream or boundary layer produces optical continuum emission and some low ionization emission lines (e.g., Lynden-Bell & Pringle 1974; Kenyon & Hartmann 1987; Bertout et al. 1988; Kenyon et al. 1996). In this picture, near-IR and optical excess emission should be correlated. For Taurus-Auriga pre-main sequence stars, there are strong correlations between IR excess emission and the optical continuum and emission lines (e.g., Hartigan et al. 1990; Hartigan 1993; Basri & Batalha 1990; Edwards et al. 1993; Valenti et al. 1993; Kenyon & Hartmann 1995).

To test for a correlation between optical and IR excess emission in Cha I sources, we collected $H\alpha$ equivalent widths, $EW(H\alpha)$, from the literature (Henize & Mendoza 1973; Appenzeller et al. 1983; Walter 1992; Gauvin & Strom 1992; Hartigan 1993; Huenemoerder et al. 1994; Alcalá et al. 1995; Lawson et al. 1996; Comerón et al. 1999). We took the average for sources with two or more measurements; using the median makes no difference in our conclusions.

Figure 4 shows the relationship between $EW(H\alpha)$ and $K - L$ for 40 sources in the SPIREX/Abu survey region with good measurements. There is a strong correlation; the Spearman rank correlation coefficient is $r_s = 0.70$. The probability that the observed distribution is drawn from a random distribution with no correlation is $p_D \approx 6 \times 10^{-7}$. As in Taurus-Auriga, all of the power in this correlation results from differences between WTTs and CTTs. The probability that the observed distribution is random increases to $p_D \approx 4 \times 10^{-5}$ for sources with $K - L \geq 0.4$ and $p_D \approx 0.13$ for sources with $K - L \geq 0.6$. Because some Cha I WTTs are heavily reddened, the division between WTTs and CTTs in Cha I occurs at a somewhat larger $K - L$ than in Tau-Aur (see Kenyon & Hartmann 1995).

As far as we know, there are insufficient measurements of $U - B$ colors or of optical or ultraviolet veiling in Cha I to attempt correlations with the IR excess emission. Nevertheless, the strong correlation between $EW(H\alpha)$ and $K - L$ indicates that accretion powers the optical emission lines in Cha I CTTs.

4. Summary

We have described an L -band photometric survey of part of the Cha I dark cloud. We detect 124 sources with $L < 11.0$, the approximate completeness limit. Our survey recovers all known pre-main sequence stars in the region and yields new measurements of near-IR excess emission in 15 candidate pre-main sequence stars from our deep JHK survey (Gómez & Kenyon 2001). The fraction of sources with near-IR excess emission is $58\% \pm 4\%$, based on a Monte Carlo simulation of the observations using an adopted reddening law. This fraction is constant for sources with $K = 9-11$.

Cha I sources have bluer $K - L$ colors than pre-main sequence stars in Taurus-Auriga. The $H - K$ colors are also bluer, despite the larger apparent reddening of some Cha I WTTs. Optical spectra are needed to derive spectral types and estimate the reddening for these sources. Accurate values for the optical extinction A_V would provide a better test of the difference between the near-IR colors for Cha I pre-main sequence stars and young stars in other clouds.

We find a strong correlation between $EW(H\alpha)$ and $K - L$ for ~ 40 Cha I sources. Stars with $K - L \leq 0.6$ have weak $H\alpha$ emission; stars with $K - L \geq 0.6$ have strong $H\alpha$ emission. This result agrees with predictions of accretion disk models, where a disk produces the near-IR excess and an accretion stream or boundary layer produces an optical/ultraviolet continuum and strong emission lines. There is weak evidence that the median $EW(H\alpha)$ is smaller for these Cha I sources than for

pre-main sequence stars in the Taurus-Auriga cloud. Magnetic accretion disk models, where the stellar magnetic field truncates the disk above the stellar photosphere, predict a smaller median $\text{EW}(\text{H}\alpha)$ for sources with bluer $K - L$ colors (Kenyon et al. 1996). If these trends for Cha I sources are correct, these data provide weak evidence for smaller accretion rates among Cha I CTTs than among Taurus-Auriga CTTs. Optical spectra for the remaining 80 stars in this Cha I field would yield a definitive test of these trends.

We are grateful to the SPIREX/Abu staff, especially C. Kaminski and K. M. Merrill, for acquiring the observations and for assistance with planning a successful observing strategy. A. Fowler and N. Sharpe from NOAO modified the Abu system for use at the South Pole and made it operational on site. We also thank J. Kastner and collaborators for performing the initial data reduction of the SPIREX/Abu images. D. Mink kindly assisted us with the WSCTools software. We thank J. Kastner, C. Lada, W. Lawson (the referee), and K. M. Merrill for helpful comments and questions.

REFERENCES

- Alcalá, J. M., Krautter, J., Schmitt, J. H. M. M., Covino, E., Wichmann, R., & Mundt, R. 1995, *A&AS*, 114, 109
- Allen, D. A. 1972, *ApJ*, 172, L55
- Appenzeller, I., Jankovics, I., & Krautter, J. 1983, *A&A*, 53, 291
- Barsony, M., Kenyon, S. J., Lada, E. A., Teuben, P. J. 1997, *ApJS*, 112, 109
- Basri, G., & Batalha, C. 1990, *ApJ*, 363, 654
- Baud, B., Young, E., Beichman, C. A., Beintema, D. A., Emerson, J. P., Habing, H. J., Harris, S., & Jennings, R. F. 1984, *ApJ*, 278, L53
- Bertout, C., Basri, G., & Bouvier, J. 1988, *ApJ*, 330, 350
- Bessell, M. S., & Brett, J. M. 1988, *PASP*, 100, 1134
- Burrows, C. J., Stapelfeldt, K. R., Watson, A. M., Krist, J. E., Ballester, G. E., Clarke, J. T., Crisp, D., Gallagher, J. S., III, Griffiths, R. E., Hester, J. J., Hoessel, J. G., Holtzman, J. A., Mould, J. R., Scowen, P. A., Trauger, J. T., & Westphal, J. A. 1996, *ApJ*, 473, 437
- Cambrésy, L., Copet, E., Epchtein, N., de Batz, B., Borsenberger, J., Fouqué, P., Kimeswenger, S., & Tiphéne, D. 1998, *A&A*, 338, 977
- Chiang, E. I., & Goldreich, P. 1997, *ApJ*, 490, 368
- Comerón, F., Rieke, G. H., Burrows, A., & Rieke, M. J. 1993, *ApJ*, 416, 185
- Comerón, F., Rieke, G. H., & Neuhäuser, R. 1999, *A&A*, 343, 477
- Edwards, S., Strom, S. E., Hartigan, P., Strom, K. M., Hillenbrand, L. A., Herbst, W., Attridge, J., Merrill, K. M., Probst, R., & Gatley, I. 1993, *AJ*, 106, 372
- Elias, J. 1978, *ApJ*, 224, 453
- Feigelson, E. D., Casanova, S., Montmerle, T., & Guibert, J. 1993, *ApJ*, 416, 623
- Feigelson, E. D., & Kriss, G. A. 1989, *ApJ*, 338, 262
- Fowler, A. M., Sharp, N., Ball, W., Schinckel, A., Ashley, M. C., Boccas, M., Storey, J. W., DePoy, D. L., Martini, P., Harper, A., Marks, R. 1998, *SPIE proceedings*, 3354, 1170
- Gauvin, L. S., & Strom, K. M. 1992, *ApJ*, 385, 217
- Ghez, A. M., White, R. J., & Simon, M. 1997, *ApJ*, 490, 353

- Glass, I. S. 1979, MNRAS, 187, 305
- Gómez, M., & Kenyon, S. J. 2001, AJ, 121, No. 2
- Haisch., K. E., Lada, E. A., & Lada, C. J. 2000, AJ, 120, 1396
- Haisch., K. E., Lada, E. A., & Lada, C. J. 2001, AJ, in press
- Hartigan, P. 1993, AJ, 105, 1511
- Hartigan, P., Hartmann, L., Kenyon, S., Strom, S. E., & Skrutskie, M. F. 1990, ApJ, 354, L25
- Hartmann, L., Calvet, N., Gullbring, E., & D'Alessio, P. 1998, ApJ, 495, 385
- Hartmann, L., & Kenyon, S. J. 1990, ApJ, 349, 190
- Hartmann, L., & Kenyon, S. J. 1996, ARA&A, 34, 207
- Henize, K. G., & Mendoza, E. E. 1973, ApJ, 180, 115
- Huenemoerder, D. P., Lawson, W. A., & Feigelson, E. D. 1994, MNRAS, 271, 967
- Hyland, A. R. 1980, in *Infrared Astronomy, IAU Symp. No. 96*, edited by C. D. Wynn-Williams & D. P. Cruikshank, Reidel, Dordrecht, p. 125
- Hyland, A. R., Jones, T. J., & Mitchell, R. M. 1982, MNRAS, 201, 1095
- Kenyon, S. J., & Hartmann, L. 1987, ApJ, 323, 714
- Kenyon, S. J., & Hartmann, L. 1995, ApJS, 101, 117
- Kenyon, S. J., Lada, E. A., & Barsony, M. 1998, AJ, 115, 252
- Kenyon, S. J., Yi, I., & Hartmann, L. 1996, ApJ, 462, 439
- Koerner, D. W., Sargent, A. I., & Beckwith, S. V. W. 1993, ApJ, 408, 93
- Krist, J. E., Stapelfeldt, K. R., Ménard, F., Padgett, D. L., & Burrows, C. J. 2000, ApJ, 538, 793
- Lada, C. J. 1999, in *The Physics of Star Formation and Early Stellar Evolution*, edited by C. J. Lada & N. Kylafis, Dordrecht, Kluwer, p. 143
- Lada, C. J., Muench, A. A., Haisch, K. E. Jr., Lada, E. A., Alves, J. F., Tollestrup, E. V., Willner, S. P. 2000, AJ, 120, 3162
- Lawson, W. A., Feigelson, E. D., & Huenemoerder, D. P. 1996, MNRAS, 280, 1071
- Lynden-Bell, D., & Pringle, J. E. 1974, MNRAS, 168, 603

- Nordh, L., Olofsson, G., Abergel, A., Andre, P., Blommaert, J., Bontemps, S., Boulanger, F., Burgdorf, M., Cesarsky, C. J., Cesarsky, D., Copet, E., Davies, J., Falgarone, E., Hultgren, M., Kaas, A. A., Lagache, G., Montmerle, T., Perault, M., Persi, P., Prusti, T., Puget, J. L., & Sibille, F. 1996, *A&A*, 315, L185
- Oasa, Y., Tamura, M., & Lawson, W. A. 1999, *ApJ*, 526, 336
- Olofsson, G., Hultgren, M., Kaas, A. A., Bontemps, S., Nordh, L., Abergel, A., André, P., Boulanger, F., Burgdorf, M., Casali, M. M., Cesarsky, C. J., Davies, J., Falgarone, E., Montmerle, T., Perault, M., Persi, P., Prusti, T., Puget, J. L., & Sibille, F. 2000, *A&A*, 357, 1020
- Persi, P., Marenzini, A. R., Kaas, A. A., Olofsson, G., Nordh, L., & Roth, M. 1999, *AJ*, 117, 439
- Persi, P., Marenzini, A. R., Olofsson, G., Kaas, A. A., Nordh, L., Hultgren, M., Abergel, A., André, P., Bontemps, S., Boulanger, F., Burgdorf, M., Casali, M. M., Cesarsky, C. J., Copet, E., Davies, J., Falgarone, E., Montmerle, T., Perault, M., Prusti, T., Puget, J. L., & Sibille, F. 2000, *A&A*, 357, 219
- Press, W. H., Flannery, B. P., Teukolsky, S. A., & Vetterling, W. T. 1992, *Numerical Recipes, The Art of Scientific Computing*, Cambridge, Cambridge
- Prusti, T., Whittet, D. C. B., & Wesselius, P. R. 1992, *MNRAS*, 254, 361
- Rucinski, S. M. 1985, *AJ*, 90, 2321.
- Rydgren, A. E., & Zak, D. S. 1987, *PASP*, 99, 141
- Schwartz, R. D. 1977, *ApJS*, 35, 161
- Schwartz, R. D., & Henize, K. G. 1983, *AJ*, 88, 1665
- Valenti, J. A., Basri, G., & Johns, C. M. 1993, *AJ*, 106, 2024
- Walter, F. M. 1992, *AJ*, 104, 758
- Wilking, B. A., & Lada, C. J. 1983, *ApJ*, 274, 698
- Wilner, D. J., Ho, P. T. P., & Rodriguez, L. F. 1996, *ApJ*, 470, L117
- Wilner, D. J., Myers, P. C., Mardones, D., & Tafalla, M. 2000, *ApJ*, 544, L69

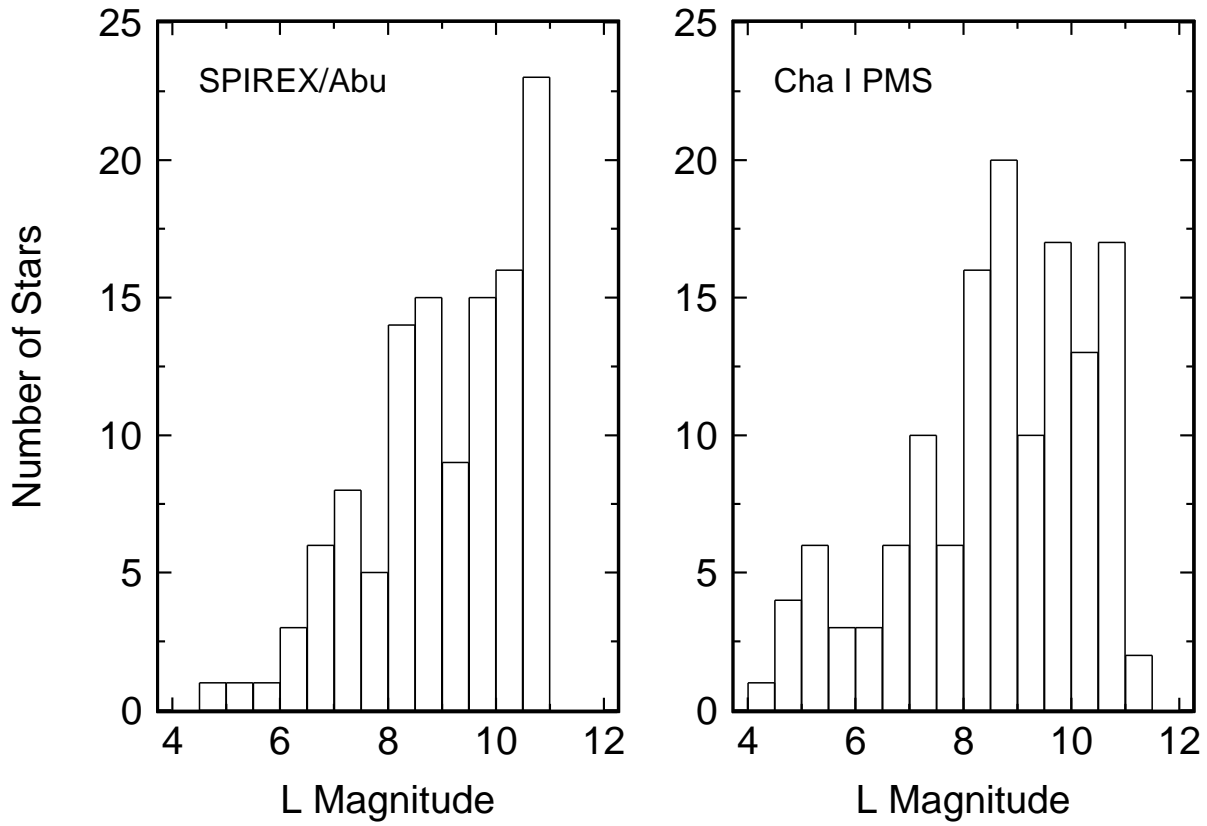


Fig. 1.— Number counts of Cha I sources. Left panel: SPIREX/Abu sources from this paper. Right panel: Known pre-main sequence stars in Cha I.

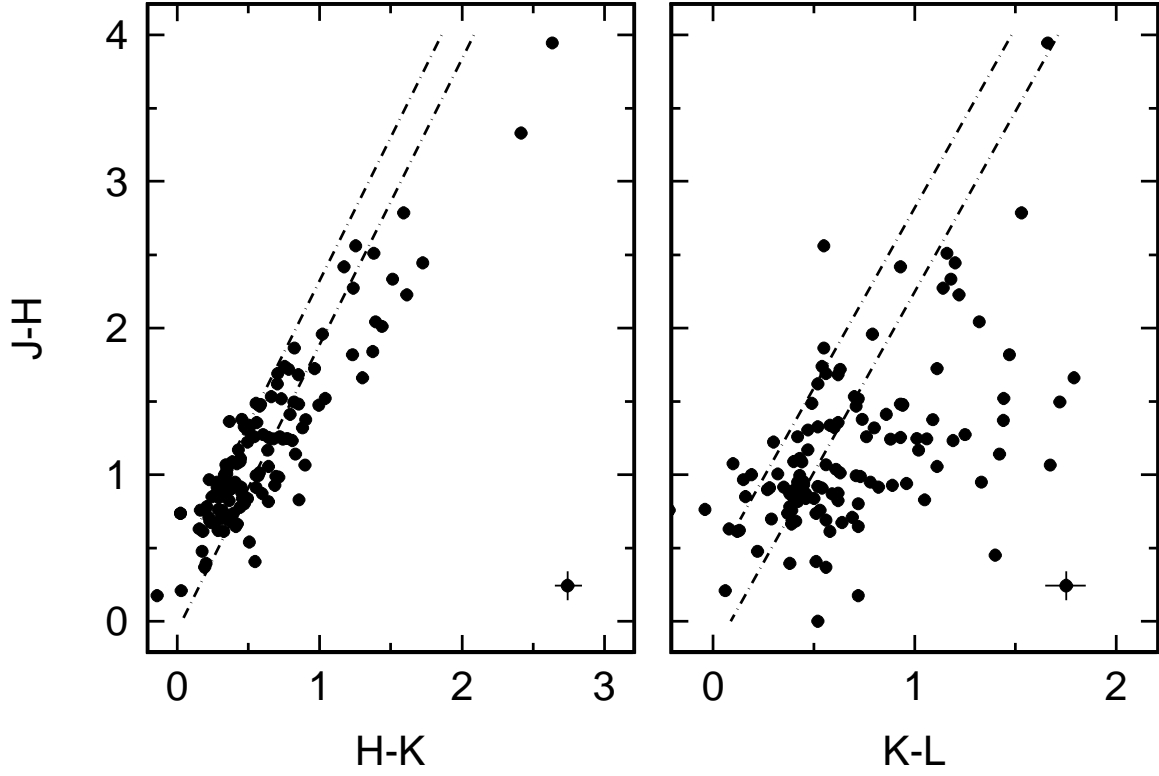


Fig. 2.— Near-infrared color-color diagrams for SPIREX/Abu survey. Left panel: $J - H$ vs $H - K$. Right panel: $J - H$ vs $K - L$. The dot-dashed lines in each panel bracket the expected locus of reddened colors of main sequence stars (Bessell & Brett 1988). The error bar in the right corner of each panel indicates 1σ errors for each color.

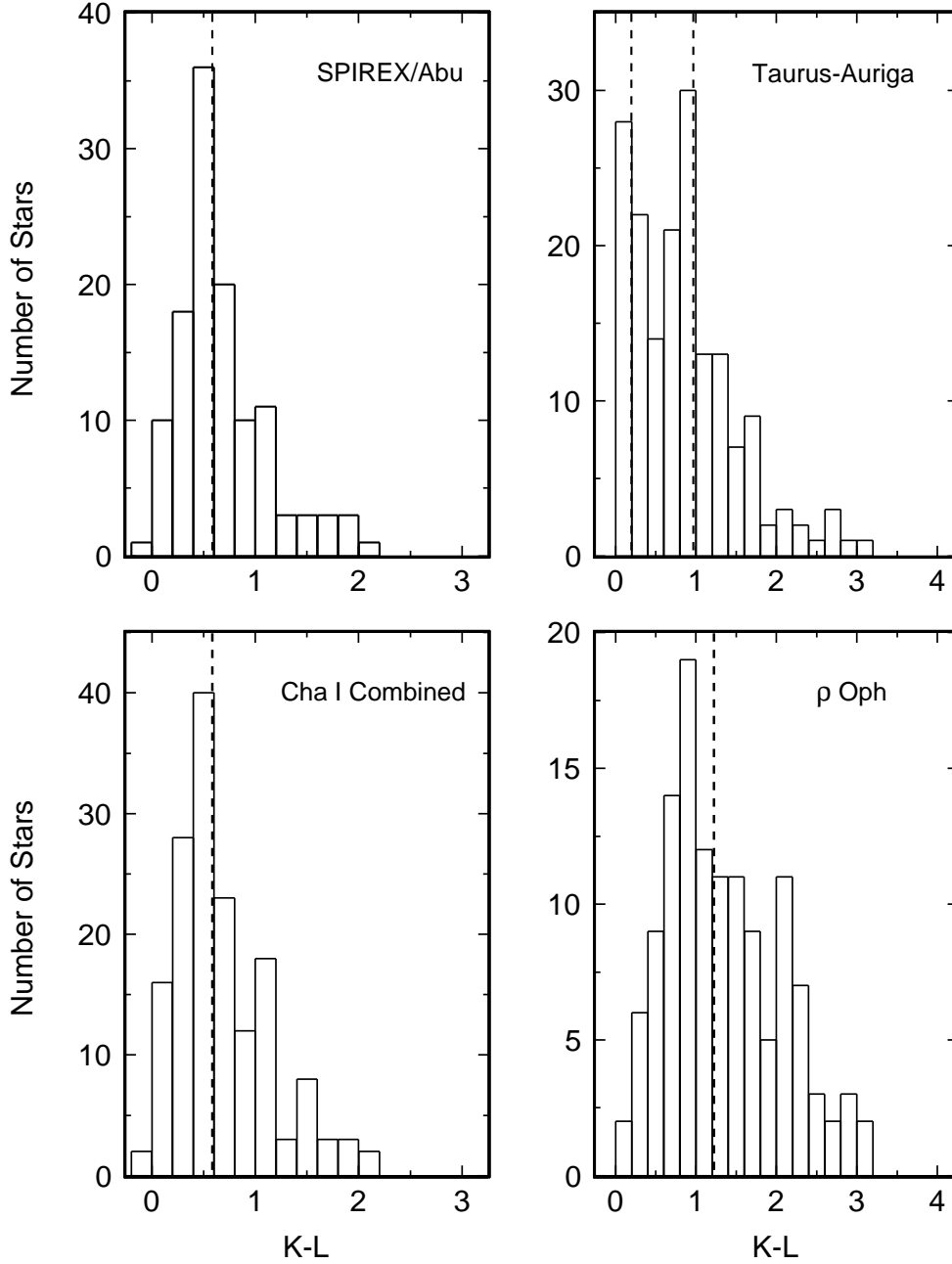


Fig. 3.— Frequency histograms for the $K - L$ color in the Cha I, ρ Oph, and Taurus-Auriga dark clouds. Upper left panel: Cha I SPIREX/Abu sample. Lower left Panel: Cha I combined sample. Upper right panel: Taurus-Auriga. Lower right Panel: ρ Oph, several ρ Oph stars with $K - L \geq 4$ have been excluded for clarity. The dashed lines indicate the median $K - L$ for the ρ Oph and both Cha I samples. In Taurus-Auriga, the dashed lines mark the median $K - L$ colors for WTTs (left dashed line) and for CTTs (right dashed line).

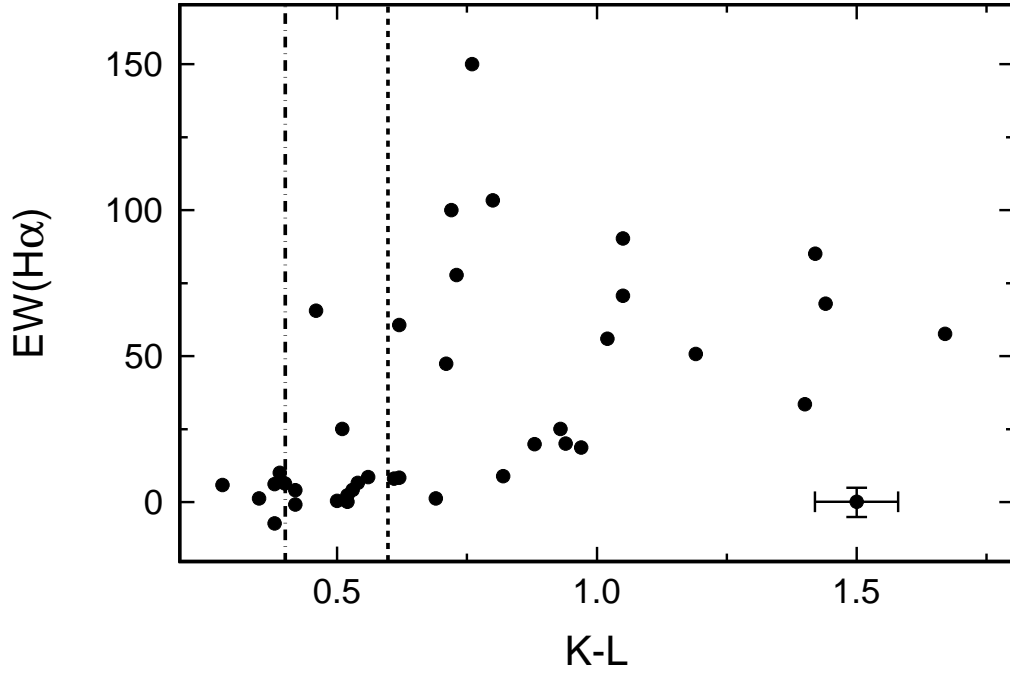


Fig. 4.— $H\alpha$ equivalent widths as a function of $K - L$ color for SPIREX/Abu sources. The dot-dashed line indicates the division at $K - L = 0.4$ between WTTs and CTTs in Taurus-Auriga. The dashed line indicates the division at $K - L = 0.6$ between reddened WTTs and CTTs in Cha I.

Table 1. *L* Band Observations for the Cha I sources

No.	$\alpha(2000.0)$	$\delta(2000.0)$	<i>L</i>	<i>K</i> – <i>L</i>	<i>H</i> – <i>K</i>	<i>J</i> – <i>H</i>	Id.	Ref.
1	11 07 11.0	–77 46 41	9.11	0.61	0.35	1.13	Hn 6, ISO 94	7,12
2	11 07 12.8	–77 43 51	9.70	0.42	0.54	1.37	CHXR 22E	4
3	11 07 16.5	–77 23 08	9.31	1.66	2.63	4.19	Denis 23, ISO 97	2,12
4	11 07 16.9	–77 26 22	sat		0.37	1.48	ISO 96	12
5	11 07 19.4	–77 29 39	9.68	0.64	0.24	0.75	ISO 99	12
6	11 07 21.6	–77 38 07	sat		0.44	0.86	Lh α 332-17, ISO 100	13, 12
7	11 07 21.7	–77 22 12	9.30	1.53	1.59	2.97	Denis 24, B 35, ISO 101	2, 1, 12
8	11 07 23.7	–77 41 25	6.90	0.74	0.45	1.49	Denis 25, ISO 102	2, 12
9	11 07 24.1	–77 42 27	10.27	0.44	0.39	1.19		
10	11 07 24.2	–77 43 50	10.72	1.11	0.64	1.15		
11	11 07 26.3	–77 01 52	10.95	–0.22	0.76			
12	11 07 28.6	–76 52 12	9.11	0.39	0.32	0.84		
13	11 07 32.3	–77 28 25	10.18	0.69	0.22	0.79	CHXR 25, ISO 105	4, 12
14	11 07 33.7	–77 11 07	9.44	0.38	0.21	0.86		
15	11 07 35.3	–77 34 51	10.55	0.40	0.34	0.98	B 34, CHXR 76, ISO 106	1, 4, 12
16	11 07 36.9	–77 35 19	9.29	0.62	0.85	1.81	Denis 26, ISO 107	2, 12
17	11 07 37.0	–77 33 33	8.52	0.70	0.66	1.65	CHXR 26, ISO 108	4, 12
18	11 07 37.5	–77 33 09	10.36	0.55	0.82	2.00	Denis 27, ISO 109	2, 12
19	11 07 38.4	–77 47 19	10.55	0.59	0.33	0.96	ISO 110	12
20	11 07 42.7	–77 34 00	9.94	0.71	0.57	1.09	H α 2, ISO 111	13, 12
21	11 07 44.5	–77 39 43	7.40	1.02	0.63	1.27	HM 15, ISO 112	8, 12
22	11 07 46.1	–77 38 05	7.33	0.93	1.17	2.59	Denis 28, ISO 113	2, 12
23	11 07 53.2	–77 36 56	10.88	0.39	0.42	0.74	H α 3, ISO 116	3, 12
24	11 07 56.7	–77 27 27	7.29	0.52	0.30	1.01	CHX 10a, ISO 117	5, 12
25	11 07 57.3	–77 41 56	8.69	0.60	0.51	1.43	ISO 118	12
26	11 07 57.5	–77 17 27	8.29	1.32	1.39	2.19	B 38	1
27	11 07 58.4	–77 42 42	8.62	1.19	0.81	1.34	Sz 23, ISO 120	13, 12
28	11 07 59.1	–77 38 46	sat		1.04	1.64	HM 16, ISO 119	8, 12
29	11 08 00.2	–77 15 33	10.38	0.72	0.47	0.89	ISO 121	12
30	11 08 00.3	–77 17 32	8.45	0.63	0.78	1.85	CHXR 30, ISO 122	4, 12
31	11 08 01.9	–77 42 29	sat		0.55	1.00	VW Cha, ISO 123	13, 12
32	11 08 03.2	–77 48 37	10.08	0.52	0.47	1.44	ISO 125	12
33	11 08 04.2	–77 38 43	sat		1.37	1.98	Denis 32, ISO 126	2, 12
34	11 08 04.2	–77 39 19	sat		0.51	0.61	HD 97048, ISO 124	12
35	11 08 10.1	–76 42 26	8.67	0.06	0.03	0.26	ISO 129	12
36	11 08 12.1	–77 18 54	9.92	0.55	1.25	2.74	Denis 33, ISO 130	2, 12
37	11 08 12.9	–77 19 13	7.74	1.16	1.38	2.68	Denis 34, ISO 131	2, 12
38	11 08 15.1	–76 37 33	9.94	0.56	0.19	0.43	ISO 133	12
39	11 08 16.4	–77 33 53	sat		0.71	1.08	Glass I, ISO 135	6, 12
40	11 08 16.9	–77 44 37	9.71	0.42	0.28	0.97	HM 19, ISO 136	8, 12
41	11 08 17.4	–77 44 11	10.19	0.51	0.39	0.82	ISO 137	12
42	11 08 20.6	–77 39 19	10.52	0.56	0.36	0.77	H α 4	3
43	11 08 20.7	–76 56 55	9.97	0.27	0.37	0.99	ISO 139	12
44	11 08 20.7	–77 05 22	10.71	0.15	0.23	1.06	ISO 140	12
45	11 08 22.6	–77 30 28	10.67	0.43	0.55	1.09	ISO 143	12
46	11 08 23.9	–76 24 06	10.50	0.08	0.16	0.70		
47	11 08 24.7	–77 41 47	9.94	0.82	0.43	1.01	H α 5, ISO 144	3, 12
48	11 08 25.8	–76 48 33	6.69			0.82		
49	11 08 38.7	–77 43 51	6.60	1.47	1.23	1.96	IR-Neb, ISO 150	14, 12

Table 1—Continued

No.	$\alpha(2000.0)$	$\delta(2000.0)$	L	$K - L$	$H - K$	$J - H$	Id.	Ref.
50	11 08 39.2	-77 16 05	8.22	0.80	0.88	1.43	HM 20, ISO 151	8, 12
51	11 08 39.6	-77 34 17	10.58	0.46	0.49	0.92	H α 6, ISO 152	3, 12
52	11 08 41.1	-76 36 08	8.92	0.28	0.36	1.00	CHX 13a, ISO 153	5, 12
53	11 08 51.5	-76 28 21	11.12	0.13	0.29	0.70	ISO 158	12
54	11 08 51.5	-76 25 12	10.53	0.72	0.41	0.72	Sz 28, ISO 157	13, 12
55	11 08 54.3	-76 49 29	11.13	0.41	0.23	0.76	ISO 159	12
56	11 08 54.6	-77 32 12	10.55	0.62	0.36	0.91	CHXR 78C, ISO 160	4, 12
57	11 08 54.7	-76 51 29	10.04	0.16	0.24	0.94	ISO 163	12
58	11 08 55.1	-77 02 13	8.13	1.42	0.83	1.24	VY Cha, ISO 162	13, 12
59	11 08 55.4	-76 32 43	10.90	0.46	0.60	0.96	ISO 165	12
60	11 08 55.4	-76 47 44	10.96	0.29	0.30	0.78	ISO 161	12
61	11 08 55.6	-77 04 52	7.04	0.56	0.34	1.17	ISO 166	12
62	11 08 56.2	-77 27 12	10.51	1.06	0.67	1.35	ISO 167	12
63	11 08 56.6	-77 31 53	8.01	0.40	0.29	0.93	ISO 168	12
64	11 08 57.2	-77 43 28	9.77	1.79	1.30	1.79	Denis 35	2
65	11 08 58.6	-77 33 57	10.94	0.78	0.28	1.04		
66	11 08 58.8	-76 46 39	10.77	0.04	0.29	0.84	ISO 170	12
67	11 09 03.8	-77 00 51	8.09	0.32	0.35	1.10	ISO 172	12
68	11 09 04.3	-77 01 53	10.75	0.40	0.44	1.19	ISO 173	12
69	11 09 04.4	-77 07 45	8.86	0.45	0.32	1.04		
70	11 09 08.2	-76 18 14	6.04	0.58	0.33	0.69		
71	11 09 08.5	-76 49 13	10.42	0.42	0.64	0.90	ISO 177	12
72	11 09 11.4	-76 32 50	10.75	1.11	0.96	1.86	Denis 36, NIR 2	2, 10
73	11 09 12.0	-77 39 06	9.91	0.56	0.71	1.82	Denis 37, ISO 179	2, 12
74	11 09 12.3	-77 29 12	8.14	0.53	0.19	0.84	Sz 30, ISO 182	13, 12
75	11 09 14.4	-76 28 40	10.28	0.51	0.55	0.47	Hn 8	7
76	11 09 15.4	-76 21 58	10.60	0.12	0.19	0.69		
77	11 09 18.3	-76 27 58	8.34	0.35	0.28	1.01	CHXR 37, ISO 185	4, 12
78	11 09 18.5	-77 47 40	7.09	0.72	-0.14	0.23	ISO 187	12
79	11 09 19.0	-76 30 30	7.88	0.94	1.00	1.59	Hn 9, ISO 186	7, 12
80	11 09 21.3	-77 36 54	11.26	0.58	0.50	1.45		
81	11 09 21.9	-77 13 58	8.15	0.47	0.43	1.27	ISO 188	12
82	11 09 23.5	-76 34 32	7.30	1.22	1.61	2.39	C1-6, ISO 189, NIR 10	9, 12, 10
83	11 09 24.3	-76 23 22	sat			0.91	VZ Cha	13
84	11 09 25.9	-77 26 25	8.63	0.71	0.58	1.59	ISO 190	12
85	11 09 26.9	-76 33 33	9.38	0.79	1.02	2.10	Denis 40, NIR 13	2, 10
86	11 09 27.3	-77 36 52	10.40	0.42	0.41	1.04		
87	11 09 29.4	-76 33 28	8.32	3.86	2.42	3.55	Denis 41, ChaNa2 #1, ISO 192, NIR 15	2, 11, 12, 10
88	11 09 31.8	-76 30 36	10.37	1.01	0.77	1.35	ISO 193	12
89	11 09 37.4	-77 26 37	10.17	0.49	0.55	1.61	ISO 195	12
90	11 09 38.0	-77 10 41	8.59	0.52	0.70	1.75	Denis 42, ISO 196	2, 12
91	11 09 39.7	-76 52 26	10.50	0.47	0.49	1.42	ISO 197	12
92	11 09 39.7	-76 28 38	8.55	0.38	0.29	0.96	CHX 15b, ISO 198	5, 12
93	11 09 41.8	-76 34 59	8.45	1.18	1.51	2.50	C1-25, ISO 199, NIR 19	9, 12, 10
94	11 09 42.1	-76 51 11	10.78	0.72	0.73	1.64		
95	11 09 43.0	-77 25 58	9.55	0.93	0.64	1.36	C7-1, ISO 200	9, 12
96	11 09 45.1	-77 40 32	10.03	0.44	0.45	1.00	ISO 201	12
97	11 09 46.2	-76 34 47	9.20	0.76	0.72	1.37	Hn 10, ISO 204, NIR 24	7, 12, 10
98	11 09 46.2	-76 28 57	7.47	0.38	0.20	0.46	CHX 15a, ISO 205	5, 12

Table 1—Continued

No.	$\alpha(2000.0)$	$\delta(2000.0)$	L	$K - L$	$H - K$	$J - H$	Id.	Ref.
99	11 09 46.8	–76 43 54	9.51	0.63	0.58	1.11	C2-3, ISO 203	9, 12
100	11 09 47.7	–76 34 06	10.72	1.14	1.24	2.43	Denis 44, C1-22, NIR 25	2, 9, 10
101	11 09 47.9	–77 26 30	8.58	1.72	0.82	1.62	B 43, ISO 207	1, 12
102	11 09 49.3	–77 31 20	10.62	0.45	0.38	1.02		
103	11 09 49.9	–76 36 49	6.85				HD 97300, ISO 2	211
104	11 09 50.6	–77 45 48	8.10	1.25	0.60	1.38	ISO 214	12
105	11 09 51.5	–76 58 57	8.54	0.22	0.17	0.54	ISO 213	12
106	11 09 52.0	–76 39 12	10.76	0.89	0.69	1.02	ISO 217	12
107	11 09 52.4	–76 57 58	9.78	0.30	0.49	1.33	ISO 216	12
108	11 09 53.3	–77 45 40	7.92	0.16	0.42	1.17	ISO 222	12
109	11 09 53.7	–76 34 26	sat		1.44	2.16	HM 23, ISO 223, NIR 27	8, 12, 10
110	11 09 53.9	–76 29 25	8.22	0.88	0.74	1.35	Sz 33, CHX 15, ISO 224	13, 5, 12
111	11 09 55.0	–76 32 40	8.05	1.20	1.73	2.61	C1-2, ISO 226, NIR 8	9, 12, 10
112	11 09 56.7	–77 18 26	9.33	0.54	0.75	1.87	Denis 47, ISO 227	2, 12
113	11 09 58.5	–76 59 15	8.51	0.43	0.44	1.21	ISO 229	12,
114	11 09 58.9	–77 37 09	6.95	0.73	0.69	1.08	WX Cha, ISO 228	13, 12
115	11 10 00.0	–77 26 33	8.98	0.94	0.59	1.60	ISO 230	12
116	11 10 00.7	–76 34 59	sat		0.90	1.16	WW Cha, ISO 231, NIR 29	13, 12, 10
117	11 10 04.1	–76 33 28	8.27	0.93	0.85	1.60	Hn 11, ISO 232, NIR 33	7, 12, 10
118	11 10 04.9	–76 35 47	8.56	0.54	0.38	1.00	GK-1, ISO 233, NIR 35	13, 12, 10
119	11 10 07.1	–76 29 38	7.86	0.62	0.45	0.96	WY Cha, ISO 234	13, 12
120	11 10 08.8	–77 27 50	10.09	1.09	0.90	1.49	ISO 235	12
121	11 10 11.9	–76 35 31	7.69	0.86	0.79	1.53	Denis 48, ISO 237, NIR 45	2, 12, 10
122	11 10 13.3	–77 27 11	9.85	0.62	0.56	1.47	ISO 239	12
123	11 10 30.5	–77 36 06	9.59	0.19	0.33	1.09	ISO 243	12
124	11 10 39.2	–77 32 42	7.38	0.50	0.46	0.92	CHXR 47, ISO 251	4, 12

Note. — Units of right ascension are hours, minutes, and seconds, and units of declination are degrees, arcminutes, and arcseconds. Sources with saturated detections on the SPIREX/Abu images are indicated by ‘sat’.

References. — (1) Baud et al. (1984), (2) Cambrésy et al. (1998), (3) Comerón et al. (1999), (4) Feigelson et al. (1993), (5) Feigelson & Kriss (1989), (6) Glass (1979), (7) Hartigan (1993), (8) Henize & Mendoza (1973), (9) Hyland et al. (1982), (10) Oasa et al. (1999), (11) Persi et al. (1999), (12) Persi et al. (2000), (13) Schwartz (1977), (14) Schwartz & Henize (1983)